Singlet-assisted diffusion-NMR (SAD-NMR): extending the scope of diffusion tensor imaging via singlet NMR

Giulia Melchiorre, Francesco Giustiniano, Sundeep Rathore and Giuseppe Pileio*

School of Chemistry, University of Southampton, SO17 1BJ, Southampton, U.K

Abstract

Long-lived nuclear singlet order methods are here combined with diffusion tensor imaging with the purpose of characterizing the full diffusion tensor of molecules that freely diffuse in large pores of up to the millimeter. Such sizes are out-of-reach to conventional diffusion tensor imaging because of the limitations imposed by the relaxation decay constant of the longitudinal magnetization. A singlet-assisted diffusion tensor imaging methodology able to circumvent such limitations is discussed and the new possibilities it offers are demonstrated through simulation and experiments on plastic phantoms containing cylindrical channels of one-millimeter diameter.

Keywords

Diffusion NMR; Diffusion tensor imaging; Long-lived spin states; Singlet spin order, Nuclear Magnetic Resonance.

*corresponding author: g.pileio@soton.ac.uk

1. Introduction

Brownian diffusion is a kind of molecular translational motion in which molecules travel through space in a random way as dictated by intermolecular collisions, thermal energy and the structural boundaries of the space they travel within. Measurements of such motion can be used to deduce important information on the diffusing species itself as well as on its surroundings (1, 2). The most basic measurable to characterize such motion is certainly the molecular self-diffusion coefficient, a quantity that measures the extent of molecular translation through Brownian motion in an isotropic space. Molecular diffusion (from now on the prefix "self" is dropped but implied all the times we refer to diffusion in this paper), however, is not always isotropic as, for example, when the size and shape of a container imposes confinement on molecules that move within or when molecules retain some sort of positional order as in a liquid crystalline phase. To characterize those situations, two quantities, namely the structural length, l_S, and the diffusion length, l_D, are commonly introduced. l_s

reports about the average dimension of the confinement, for example, the average diameter of spherical pores or the average length of channels in a structure, whereas l_D represents the average distance travelled by the molecules during the diffusion time Δ, also known as the root mean square displacement, $l_D = \sqrt{2D\Delta}$, with D representing the diffusion coefficient. These quantities are of particular importance in the study of porous media, which are heterogeneous materials characterized by a matrix hosting a network of voids, called pores. The size and shape of such pores can indeed restrict molecular diffusion so that the diffusive motion itself becomes anisotropic, i.e. different when measured along different directions of space. In those systems (and many others), it is generally more correct to discuss diffusion in terms of a diffusion tensor and referring to the isotropic diffusion coefficient as the trace of the diffusion tensor. As discussed below, the diffusion tensor can also be diagonalised to reveal the principal directions of diffusion (the tensor eigenvectors) and the diffusion coefficients along those principal directions (the tensor eigenvalues).

Molecular diffusion can be encoded within nuclear magnetic resonance (NMR) experiments (1) and NMR measurements of diffusion have already been used to obtain a plethora of molecular and structural information on a variety of systems which spans all the way from material sciences (rocks, bones, etc) to medicine (blood cells, intercellular space, brain fibers) (3-10). In particular, and relevant to this paper, the full diffusion tensor can be measured using the magnetic resonance technique known as diffusion tensor imaging (DTI) (11). In DTI, the full diffusion tensor is reconstructed after measuring molecular diffusion along a minimum of six directions chosen so to evenly probe the space around the molecule (11-13). There are many spectacular applications of the DTI technique in the medical *in-vivo* field, the most striking one is perhaps brain tractography (12, 14, 15).

All magnetic resonance based diffusion methods (the most famous of which are based on the pulsed-gradient spin echo (PGSE) or pulsed-gradient stimulated spin echo (PGSTE) pulse sequences) have a common approach: a pulsed magnetic field gradient (PFG) imposes a difference in the spins' Larmor frequency along a given direction, thus marking molecular positions' along that direction of space; successively, molecules (and the spins they carry) undergo Brownian motion for a given time interval, called the diffusion time; finally, a further PFG "reads out" the new molecular position revealing the extent of diffusive motion they undertook in a change of signal intensity. It is therefore evident that the positional information encoded by the first PFG must survive throughout the diffusion time to be decoded by the second PFG. Most typically, NMR-encoded information lives for a maximum time which is

of the order of T_1, the relaxation decay constant of longitudinal spin order. Therefore, T_1 sets a limit to the diffusion timescale and, hence, to the diffusion space-scale. Important structural information *remains hidden,* or *wrong conclusion* can be drawn, if molecules are not allowed to *properly* explore the surrounding space. In DTI, for example, diffusion would still appear isotropic (the same diffusion coefficient in all directions) even when molecules diffuse in an highly anisotropic structure made by long and narrow channels, if T_1 only allows molecules to move for an average distance which is smaller than the smallest spatial dimension of the space they are filling. With a typical T_1 value of seconds and a diffusion coefficient of the order of 10^{-9} m^2 s^{-1}, molecules usually travel an average of 10-200 μm during a conventional NMR diffusion experiment. Such distance sets the maximum dimension of the structures that can be accurately studied with conventional NMR diffusion techniques.

In systems of two coupled spin-1/2 nuclei, spin order can be prepared in the form of singlet order, which is a form of nuclear spin order that survives longer than T_1, most typically by an order of magnitude or more (16). Molecules containing such spin system can therefore be used as probes of molecular diffusions in systems where motions happen on a long-timescale or over large distances. Indeed, singlet order has been already combined with NMR diffusion experiments to measure very slow-flow (17), to image diffusion over a macroscopic scale or to probe millimeter-sized confinements with q-space diffraction techniques (18), and to measure tortuosity in porous media (19). We group all these methods, where long-lived spin order is exploited in diffusion experiments, under the acronym SAD-NMR, which stands for singlet-assisted diffusion nuclear magnetic resonance.

In this paper, we discuss a further application of SAD-NMR aiming at extending the scope of conventional DTI techniques so to allow measurements of the diffusion tensor in porous structures containing millimeters-sized pores and channels.

With the intent to discuss the technique and assess its new limitations we present here experimental results obtained on 3D-printed model structures containing channels of 1 mm ID.

2. Methodology

2.1 Basics of DTI

In diffusion tensor imaging studies, molecular diffusion in anisotropic environments is described by a diffusion tensor, $\boldsymbol{D}$, which is a rank-2 tensor of the form:

$$\boldsymbol{D} = \begin{pmatrix} D_{xx} & D_{xy} & D_{xz} \\ D_{xy} & D_{yy} & D_{yz} \\ D_{xz} & D_{yz} & D_{zz} \end{pmatrix} \qquad (1)$$

The diffusion tensor is symmetric ($D_{ij} = D_{ji}$) and therefore only contains six independent values, $D_{xx}, D_{xy}, D_{xz}, D_{yy}, D_{yz}, D_{zz}$. These values can be measured, and the full tensor characterized, if molecular diffusion is measured along, at least, six independent directions in space.

The diffusion coefficients along any given direction, is routinely measured in NMR using one of the many pulse sequences developed over the years, the most basic of them being the pulsed-gradient spin echo cited above. Modifications of this experiment introduced in order to prolong the diffusion time (PGSTE), correct for eddy currents (PGSTEbp), and compensate for thermal convection (PGdSTE and PGdSTEbp) have been available for years and are largely used by the NMR community (1). The results obtained in this work, could be compared with those acquired using the PGSTEbp pulse sequence (see Figure 1a) that gives access to the longest diffusion time among all conventional (i.e., non-singlet-based) DTI techniques. As derived by Stejskal & Tanner (20), the PGSTE experiments produces an NMR signal whose intensity follows the equation:

$$S = S_0 \, e^{-\gamma^2 g_\alpha^2 \delta^2 D_\alpha \left(\Delta - \frac{\delta}{3}\right)} \qquad (2)$$

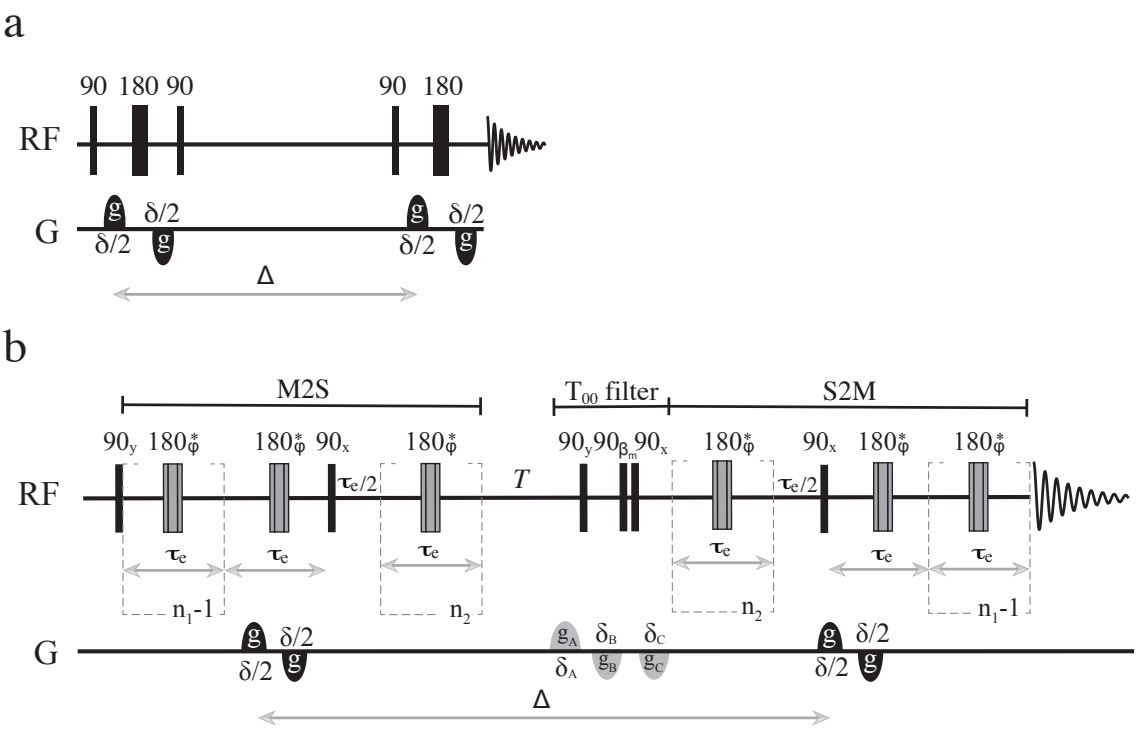

Figure 1. A sketch of a) the pulsed field gradient stimulated echo pulse sequence with bipolar gradients (PFG-STEbp); and b) the singlet-assisted diffusion pulse sequence with bipolar gradients and singlet order filter. $n_1 = \pi J/(2\Delta\nu)$ *and* $n_2 = n_1/2$. $\tau_e = 1/\left(2\sqrt{J^2 + \Delta\nu^2}\right)$. β_m *indicates the magic angle and * indicates a composite 180° pulse built as* $90_x180_y90_x$ *and with overall phase* ϕ *cycled within each echo train as* $[x, x, \bar{x}, \bar{x},\ \bar{x}, x, x, \bar{x}, \bar{x}, \bar{x}, x, x, x, \bar{x}, \bar{x}, x]$.

The signal is a function of the direction (α), total duration (δ) and strength (g_α) of the gradient, the diffusion time (Δ) and the diffusion coefficient along that direction (D_α). S_0 is the signal when $g_\alpha = 0$. Most commonly, once a direction is chosen, the diffusion time is fixed and a series of experiments is performed by changing the gradient strength while keeping its duration fixed within the limit $\delta \ll \Delta$ (the condition under which Eq. 2 was derived). Alternatively, it is possible to fix the strength and vary the duration or fix both strength and duration and vary the diffusion time. In order to derive the diffusion coefficient along the $\alpha - th$ direction, Eq. 2 is fitted to the areas of the acquired NMR peaks.

To reconstruct the whole diffusion tensor, the PGSTEbp experiment (or any alternative) is run along (at least) $n_d = 6$ independent directions. To interpret the whole data set when multiple directions are chosen, the equation for the NMR signal is rewritten as:

$$S_{g_\alpha} = S_0\, e^{-\gamma^2\delta^2 g_\alpha^2\left(\Delta - \frac{\delta}{3}\right)\alpha^T \boldsymbol{D}\alpha} \qquad (3)$$

where $\alpha = \{\alpha_x, \alpha_y, \alpha_z\}$ now indicates a unit vector that specifies the direction of space along which the pulsed field gradient is applied, and the superscript ^{T} indicates its transpose.

Note that, the choice of the six directions along which diffusion is measured and the diffusion tensor is reconstructed from, is arbitrary so long as they are independent of each other. However, it is best if these directions are chosen so to sample the 3D space as uniformly as possible (21). The number of directions can also be increased to more than six but this improves accuracy at the expense of experimental time. If the gradient strength is incremented in n_g steps per direction, a total number of $n_d * n_g$ experimental signal areas will be available. The linearized version of Eq. 3 results in a linear system of $n_d * n_g$ equations that can be matched to the experimental signal areas and solved simultaneously to yield the six unknown components of the diffusion tensor. The diffusion tensor so reconstructed is expressed in the laboratory frame since the gradient pulses are applied along the laboratory frame directions.

The diffusion tensor is diagonalized to obtain its principal values ($D'_{xx}, D'_{yy}, D'_{zz}$) and principal axes ($X', Y', Z'$) as the eigenvalues and eigenvectors of the tensor, respectively. The principal values represent the extent of diffusion along the principal directions. The orientation of the principal frame with respect to the laboratory frame (always expressible in terms of 3 Euler angles) can give insight of the existence, orientation, and geometry of compartments where diffusion is facilitated in some directions rather than others. This is conveniently captured by drawing the ellipsoid that describe the principal diffusion tensor. Such ellipsoid has its three main axes pointing along the three principal directions (eigenvectors) whilst the elliptic radius along those principal directions is equal (or proportional) to the corresponding eigenvalue. The whole procedure is here summarized in Figure 2.

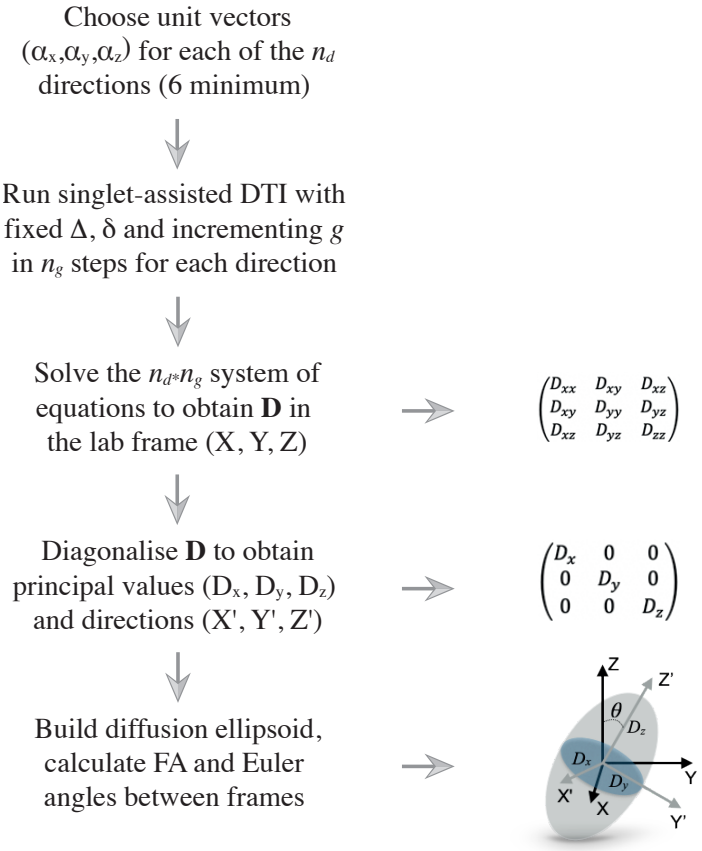

Figure 2. A flow diagram of the DTI procedure. The left column shows the logical flow of operations that start from the choice of the directions along which the diffusion is measured and lead to the processing of the results which is typically rendered in terms of a diffusion ellipsoid and its fractional anisotropy. The right column shows some details of the various steps.

If diffusion is identical in all directions of the space, the diagonal diffusion tensor has 3 identical eigenvalues and its associated ellipsoid is, in fact, a sphere. If diffusion is equal in two directions and faster in the third one, the ellipsoid is prolate with its main axis pointing along the direction of faster diffusion. Similar reasoning can be used for other cases. A crucial point to take into consideration, is that the shape of the ellipsoid can be connected to the shape of the container inside which diffusion is happening (the pores or channels inside a porous medium, for example). However, for the confinement to become influential, and its structural features to be correctly reflected by the diffusion ellipsoid, molecules need to diffuse far enough to feel the restrictions of the container. Recalling the structural and diffusion length previously introduced, the diffusion ellipsoid would appear spherical whenever $l_D \ll l_S$. Since for a given molecule diffusing in a structure both D and l_S are fixed, the parameter which is required to be adjusted in order to correctly probe the structure is the diffusion time Δ. The longer the diffusion time, the bigger the characteristic structural lengths that can be probed with

meaningful results. In this paper, we propose an alternative to the PGSTEbp experiment to get access to much longer diffusion times.

Finally, information about the shape of the diffusion tensor is often conveyed in a single index known as fractional anisotropy (FA) and calculated as (22):

$$\mathrm{FA} = \sqrt{1 - \frac{D'_{xx}D'_{yy} + D'_{xx}D'_{zz} + D'_{yy}D'_{zz}}{\left(D'_{xx}\right)^2 + \left(D'_{yy}\right)^2 + \left(D'_{zz}\right)^2}} \qquad (4)$$

The fractional anisotropy ranges from 0 to 1 with zero obtained in the case of isotropic diffusion and 1 in a fully anisotropic structure such as a thin and long channel.

2.2 Singlet-Assisted DTI

As briefly introduced above, long-lived spin order can give access to very long diffusion times. This form of order has already been exploited in this respect to measure small diffusion coefficients (23, 24) or slow flow (25). Here, we aim to combine the latest methodologies for the manipulation of this form of spin order with the more conventional DTI technique discussed above. Our proposed methodology is based on the pulse sequence reported in Figure 1b (pulse sequence code - Bruker Topspin language – is available upon request) and has been labelled as SAD-TI (singlet assisted diffusion tensor imaging). In our approach, as in PGSE and PGSTE, the well-studied (26) singlet preparation (M2S) and reading (S2M) pulse sequence blocks have been *sensitized* to molecular diffusion with the introduction of a bipolar pulsed field gradient. Namely, two opposite-in-sign field gradients are placed before and after the 180 degrees radiofrequency pulse within the first echo train of the M2S block. From that time point onwards, molecular position is encoded until a second identical bipolar gradient is applied after the diffusion time Δ as shown in Figure 1b. At the end of the M2S block, the diffusion sensitized magnetization has been converted into diffusion sensitized long-lived order which gives access to much longer diffusion times than those available with the spin-echo or stimulated-echo experiments where the diffusion encoding is done on transverse and longitudinal order, respectively. This is because the decay time constant of singlet order, T_S, is often more than an order of magnitude longer than the decay time constant of transverse order (T_2, exploited in PGSE) and longitudinal order (T_1, exploited in PGSTE). The values of n_1, n_2 and τ_e occurring in the M2S/S2M blocks are indicated in the caption of Figure 1. It is worth nothing that the minimum Δ accessible with this method is limited by the cumulative duration of the part of the M2S after the bipolar gradient, the duration of the singlet filter, and the initial

duration of the S2M until the gradient. This minimum time is of the order of some hundreds of milliseconds. Moreover, the maximum amount of initial polarization that is detectable after the sequence M2S-filter-S2M is theoretically limited to 2/3 (26) (and most practically found to be ~1/2 because of pulse imperfections and T_2-driven losses during the echo trains) and this signal loss must be weighed against the benefits of accessing a much longer timescale. in order to obtain the six independent components of the diffusion tensor in the laboratory frame within the SAD-TI experiment, Eq. (3) is fitted to the signal areas recorded in a series of experiments run at different values of the gradient strength, one set of gradient strengths for each of the (minimum) six directions, as detailed above.

2.3 Errors on diffusion tensors and related quantities

In order to estimate the errors on principal values and direction of the diffusion tensor as well as on fractional anisotropy and all other quantities, we have used a Monte Carlo approach implemented in a custom-made Mathematica notebook. Note that an analytic approach is also available (27), here not used because unfamiliar to us. The procedure runs as follows:

1. The standard deviation on each of the six independent diffusion coefficients is extracted from the fitting routine (we use *NonlinearModelFit* routine in Mathematica);
2. A new diffusion tensor is built by randomly choosing a value for each of its six components using a normal distribution centered at the parameter's best-fit value and whose standard deviation is derived in step 1
3. The new diffusion tensor is diagonalised and eigenvalues and eigenvectors are stored in separate arrays
4. The fractional anisotropy and the angle between the eigenvector corresponding to the larger eigenvalue and the z-laboratory axis is calculated and stored in separate arrays (any other quantity of interest can be derived in the same way)
5. Steps 1-4 are repeated N times (50,000 in this paper)
6. The average and the standard deviation of the arrays derived through steps 3-5 (containing N sets of eigenvalues, eigenvectors, fractional anisotropies and Euler angles) are computed and reported.

3. Materials and Methods

3.1 The molecular probe

The SAD-TI method requires a molecular probe that supports long-lived spin states so that it can travel long and far within the large channels and pores of the structure to probe its

anisotropy. In our laboratory we have custom designed a variety of probes that suites this purpose and for the current investigations we have used the molecule of 1-(ethyl-d5),4-(propyl-d7)(*Z*)-but-2-enedioate (dubbed EPM) sketched in Figure 3.

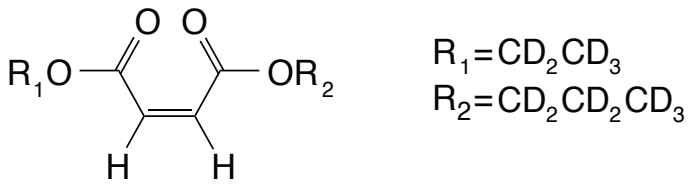

Figure 3: Molecular scheme of 1-(ethyl-d5) 4-(propyl-d7)(Z)-but-2-enedioate used in this paper as a singlet-bearing molecular probe for singlet-assisted DTI experiments

The two protons on the double bond constitutes the singlet-pair whereas all the other protons have been substituted by deuterons to minimize out-of-pair dipolar relaxation contributions and prolong the singlet lifetime. The difference in chemical shift frequency between the two protons is 3.1 ppb (0.93 Hz in our 7.04 T magnet) and their mutual scalar coupling constant is 11.9 Hz. These values qualify the magnetic properties of the molecular probe as a nearly-equivalent spin system. In such systems, singlet order is a good eigenvalue of the high-field spin Hamiltonian and remains long-lived without the need for singlet locking irradiation which would not be compatible in diffusion experiments because can generate heat and related convective flow. The isotropic diffusion coefficient for this molecule, measured in a isotropic liquid sample prepared as a 0.25 M solution of EPM in Acetone-d_6 in a 10 mm OD NMR tube, is $D_0 = 1.6 \times 10^{-9}$ m^2 s^{-1} (obtained using a standard convection compensated PGdSTEbp pulse sequence).

3.1 Structures under investigation

To demonstrate the potential of the SAD-TI methodology we aimed to measure the diffusion tensor of our probe molecule dissolved in a low-viscosity liquid and contained into the long and narrow cylindrical channels cut into the plastic structures shown in Figure 4. Both structures were machined in-house from a rod of polyoxymethylene (POM, chosen because it has good resistance to many common organic solvents and is easy to machine). The outer diameter of each structure was 7.65 mm and their length was 20 mm. Structure **00D** (Figure 4a) has 13 cylindrical channels of 1 mm diameter. The total volume of the 13 channels is 204 mm^3. The channels have their long axis oriented along the long axis of the rod, a fact that we

indicate as $\theta = 0^{\circ}$. The angle θ is intended as the angle between the channels' long axis and the rod long axis. However, the manufactured structures are aligned with their long axis parallel to the direction of the static magnetic field. Hence, θ is also the angle between the channels' long axis and the static magnetic field. Structure **30D** (Figure 4b) has 15 cylindrical channels of 1 mm diameter oriented such that their long axis makes an angle $\theta = 30^{\circ}$ with respect to the rod's long axis. The total volume of the empty channels in structure **30D** is 127 mm^3. Both plastic structures are hold within a 10 mm OD (7.8 mm ID) medium-wall LPV NMR tube. The volume of the annular cylinder arising between the tube ID and the plastic OD is 36 mm^3, molecules trapped in this region of space experience a different constriction than the molecules trapped in the cylindrical channels.

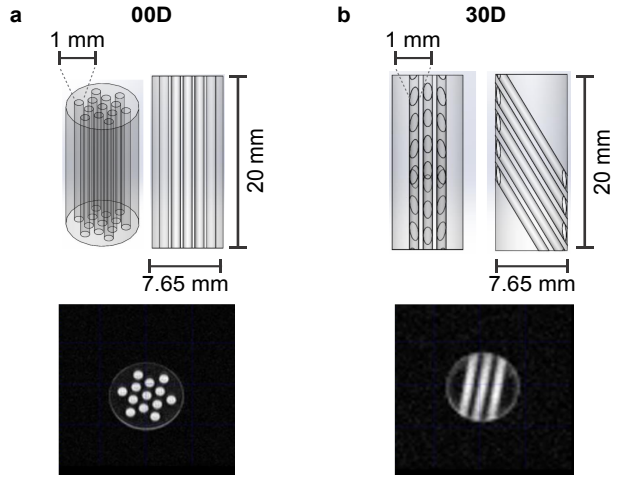

*Figure 4: Geometry and dimensions of a) **00D** and b) **30D** channel structures used for the experiments in this paper. The MRI images below were done with a multi slice multi echo (MSME) sequence (FOV 2 x 2 cm^2, 128 x 128 matrix, slice thickness 1 cm, TE = 5.08 ms). Sagittal slices (not shown) were taken to confirm that all channels were fully filled with the EPM solution.*

Structure **00D** and **30D** were imbibed with 350 µl of a 0.25 M solution of EPM in Acetone-d_6. The NMR tubes were then degassed through 10 cycles of freeze-pump-thaw to minimize the O_2 content and hence prolong relaxation times. MRI images of the tubes were taken to check all channels were properly filled up with the EPM solution (see Figure 4).

3.3 Instrumentation

All experiments were run on an Oxford Inst. 7.04 T Magnet coupled to an Avance III Bruker NMR console. The instrument is equipped with a Bruker MIC5 microimaging probe carrying a 10 mm $^{1}H/^{13}C$ resonator and a 3-axes gradient system able to deliver pulsed field gradients of up to 1.5 T m^{-1}. The samples were sitting at room temperature (21 ^{o}C) and the probe's temperature controller was turned off in order to achieve a more uniform sample temperature

and minimize convection flow, although thermal convection is already negligible given the relatively small diameter of the channels.

3.4 Numerical Simulations

This paper uses numerical simulations in comparison to experimental data. The routines developed to calculate the diffusion tensor in the structures discussed in Sec. 3.1 have been written in Mathematica (simulation code available upon request). Simulations are based on a simple random-walk approach that takes the following steps (for each structure and each value of the diffusion time):

1. The actual sample shape and geometry is reconstructed using the concept of *Region* in Mathematica
2. The experimentally measured isotropic diffusion coefficient D_0 and the diffusion time Δ used in the experiment are entered
3. The total number of molecules is set to $N_M = 10{,}000$
4. The total number of random steps is set to $N_J = 10{,}000$. This represents the number of steps that each molecule does during the diffusion time Δ, hence the time step (how long a step lasts for) is derives as $t_s = \Delta/N_J$
5. An array of N_M initial molecular position $r_i = (x_i, y_i, z_i)$ is randomly generated such that all molecules lie within the voids of the structure (i.e., within the channels and the annular cylinder forming between the tube inner wall and the plastic rod outer one)
6. Starting from r_i, the molecular position of each of the N_M molecules is propagated for the N_J steps, each step taking a length $l_s = (6\, D_0\, t_s)^{1/2}$. At each step, the new molecular positions are checked to verify they fall within the voids of the structure and, if not, a new random step is taken. This process results in an array containing all final positions $r_f = (x_f, y_f, z_f)$ for each of the N_M molecules
7. The $\alpha\beta$ component of the diffusion tensor ($D_{\alpha\beta}$) is derived as:

$$D_{\alpha\beta} = \frac{1}{2\,\Delta\,N_M}\sum_{k=1}^{N_M}\left(\alpha_{f,k} - \alpha_{i,k}\right)\left(\beta_{f,k} - \beta_{i,k}\right)$$

   with $\alpha, \beta \in [x, y, z]$, k being an index that runs on the number of molecules, and the subscripts i and f indicating the initial and final position, respectively.
8. Once the six independent $D_{\alpha\beta}$'s are calculated, the full diffusion tensor is constructed, diagonalised and parameters such as the apparent isotropic diffusion coefficient and the fractional anisotropy are calculated.

4. Results and Discussion

Before proceeding with the measurement of the diffusion tensor, we measured the decay constant of longitudinal and singlet order, T_1 and T_S respectively, for the two structures here investigated. T_1 was measured with a standard saturation recovery technique and T_S was measured with the M2S/S2M pulse sequence(28, 29). Results are summarized in Table 1. The small differences in these parameters across the two structures are within errors are most likely due to differences in the quality of the degassing procedure.

Table 1: Longitudinal and singlet order decay constants measured in the sample investigated in this paper

Sample	T_1 (s)	T_S (s)
EPM in Acetone-d_6 in **00D**	22 ± 1	230 ± 10
EPM in Acetone-d_6 in **30D**	23 ± 1	260 ± 30

The lifetime of singlet order is therefore about 13 times longer than the one of longitudinal order, in this particular case. Lifetime enhancement factors of up to 140-fold have been observed (30).

To demonstrate the advantages of the SAD-TI procedure and define its limits we have run the pulse sequence in Figure 1b on both **00D** and **30D** structures. For each structure, experiments have been repeated at 4 different values of the diffusion time Δ, namely 1.5 s, 30 s, 120 s and 240 s, with the purpose of highlighting the limits of conventional DTI against the benefits of SAD-TI. For each value of Δ, the gradient strength g was incremented in 8 steps, linearly spaced within the limits indicated in Table 2. The duration of the diffusion sensitizing gradients was kept fixed at $\delta = 320$ μs. The strengths and durations of the gradients in the T_{00} filter were $g_A = -g_B = -g_C = 45$ mT m^{-1} (3% of maximum), $\delta_A = 1.0$ ms, $\delta_B = 1.2$ ms and $\delta_C = 2.2$ ms.

Table 2. The minimum and maximum values of the gradient strength for the pulse sequence in Figure 1b expressed as a percent of the maximum gradient strength available 1.5 T m^{-1}. The last column contains the number of transients acquired and summed upon acquisition.

Δ (s)	$\boldsymbol{g_{min}}$ (% of max)	$\boldsymbol{g_{max}}$ (% of max)	Transients
1.5	1	60	2
30	1	14	4
120	1	6.5	8
240	1	4.7	16

The unit vectors for the six directions were chosen from those suggested by Jones *et al*. (21) and are summarized in Table 3.

Table 3. Unit vectors for each of the six directions used in all experiments.

	$\mathbf{d_1}$	$\mathbf{d_2}$	$\mathbf{d_3}$	$\mathbf{d_4}$	$\mathbf{d_5}$	$\mathbf{d_6}$
$\boldsymbol{\alpha_x}$	1	0.447	0.447	0.447	0.447	-0.447
$\boldsymbol{\alpha_y}$	0	0.895	0.277	-0.724	-0.724	-0.277
$\boldsymbol{\alpha_z}$	0	0	0.850	-0.525	0.525	0.850

The values of the parameters in the M2S/S2M blocks in the pulse sequence were experimentally optimized around the theoretical values and found to be: $n_1 = 20$, $n_2 = 10$ and $\tau_e = 41.8$ ms.

The results of the SAD-TI procedure are reported in Table 4. Instrumental differences of the gradient performances along different directions have been corrected by independently calibrating the gradients along each direction such that the SAD-TI experiment with $\Delta = 1.5$ s results in an exactly spherical (i.e. isotropic) tensor. This is effectively done by multiplying each of the unit vectors in Table 3 by a correction factor calculated as:

$$c_i = \frac{D_i}{\sum_{i=1}^{n_d} D_i} \qquad (5)$$

where c_i is the correction factor for the ith-direction, D_i is the diffusion coefficient measured along the ith-direction in our SAD-TI experiment with $\Delta = 1.5$ s and the term at the denominator is effectively the average diffusion coefficient along the n_d directions (6 in our case). The success of this calibration procedure results in a perfectly null FA value for the $\Delta = 1.5$ s case.

*Table 4. Experimental and simulated results of the SAD-TI procedure on **00D** and **30D** at different values of the diffusion time. The diffusion length l_D is calculated using the measured isotropic diffusion coefficient and the actual value of Δ. Differences are calculated as experimental minus simulated divided by experimental values.*

00D		**Experiments**			**Simulations**			**Difference**		
Δ (s)	l_D (μm)	D_0^a(10^{-9} m s^{-2})	FA	θ (º)	D_0^a(10^{-9} m s^{-2})	FA	θ (º)	D_0^a	*FA*	θ

1.5	70	1.66±0.04	0*	65±28	1.45	0.08	2.5	13%	-	-
30	310	1.25±0.05	0.27±0.04	0.9±3	1.17	0.27	0.8	6%	0%	11%
120	620	0.92±0.02	0.59±0.01	0.3±0.1	0.88	0.59	0.3	4 %	0%	0%
240	875	0.83±0.02	0.86±0.02	1±0.1	0.72	0.74	0.5	13%	14%	50%
30D										
1.5	70	1.65±0.03	0*	64±26	1.45	0.07	13.4	12%	-	-
30	310	1.27±0.03	0.27±0.02	29.3±2	1.17	0.27	24.7	8%	0%	16%
120	620	0.87±0.06	0.62±0.02	29.3±1	0.85	0.57	27.1	2%	8%	8%
240	875	0.72±0.02	0.84±0.02	32.0±0.4	0.72	0.69	27.0	0%	18%	16%

As expected, at very short diffusion times (of the order of a few seconds) it is not possible to catch neither the correct fractional anisotropy nor the channels' orientation with respect to the magnetic field. At modestly long diffusion times (of the order of ~$3T_1$) the channel orientation is correctly obtained although the measured fractional anisotropy is quite far from the expected value of ~0.95 for a cylinder of 1 mm radius and 20 mm length. Our numerical simulations of the diffusion tensor in the actual geometries are in quite good agreement with the experimental values despite the low level of sophistication of the model used to simulate the random walks and the relatively low number of random steps and molecules chosen. To get a correct value for the FA, a diffusion time of several minutes is required. This can be explained as follows: in order to track the channel orientation, it is just enough to find the direction associated with the largest eigenvalue of the diffusion tensor, no matter the exact value of the diffusion coefficients along each principal direction. For this reason, the channel orientation is correctly measured even at relatively short diffusion times (note that this still requires diffusion times of tens of seconds). To properly characterise the FA, the limiting value of the diffusion coefficient along each principal direction must be correctly measured and, for this to happen, one needs to use a diffusion time that allows a diffusion length of the order of the characteristic length of the structure. To further highlight the importance of the technique, we plotted the diffusion constant measured on structure **00D** along each principal direction at different values of the diffusion time, normalised to the isotropic diffusion constant (Figure 5). The plot shows that the diffusion is basically free along the z-direction (coinciding with the channels' long axis) and restricted, to an equivalent extent, along the two perpendicular directions. In a structure

with connected pores, the value of $D_{\alpha\beta}(\Delta)/D_0$ tends to $1/\alpha$ for sufficiently long diffusion time Δ, with α being the tortuosity (31), i.e. the ratio of the effective path length to the shortest path length in a porous medium. Tortuosity is therefore an indicator of pore connectivity and, as such, a fundamental quantity in understanding fluid transport through the material, for example.

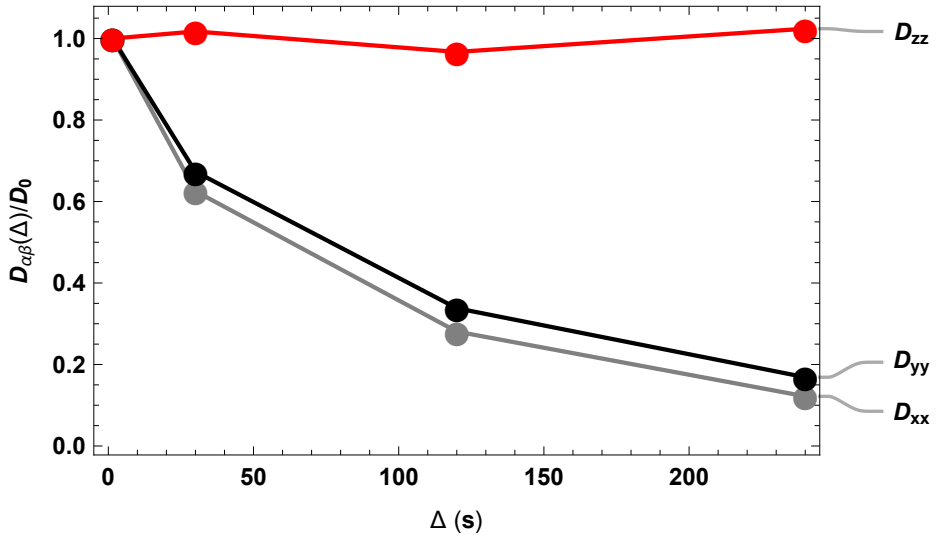

*Figure 5. The diffusion constant measured, on structure **00D**, along the three principal directions normalized to the isotropic diffusion constant and plotted versus the diffusion time Δ. The rapid drop observed in x and y principal directions reflects restricted motions in that plane. No restriction is observed in the z-principal direction since it coincides with the channel's long axis.*

Although tortuosity is not explicitly addressed in this paper, Figure 5 demonstrates how the singlet-assisted DTI technique presented here can give easy access to the value of tortuosity along the 3 principal directions of a porous medium with large pores.

In fair comparison with other technique, this same information can be accessed through conventional DTI (PGSTE based) if a molecule with very long T_1 or larger diffusion constant is available. Assuming relaxation is dominated by dipole-dipole interaction, as often the case for small molecules in non-viscous liquids, minutes-long T_1 are rare and usually linked to nuclei with low gyromagnetic ratio whose NMR sensitivity is often the limiting factor in diffusion studies within porous media. The use of gases whose self-diffusion coefficient is 4-5 order of magnitude bigger than liquids is a good alternative since the molecules can move much further even within a short diffusion time. The use of hyperpolarised-Xe was indeed proposed for diffusion studies of similar nature (32) but again the low sensitivity requires hyperpolarisation which adds a level of complication and requires specific expertise and relatively costly

equipment. Our technique can be easily implemented on conventional high-resolution NMR hardware and this constitutes a clear advantage over other techniques.

5. Conclusions

We have presented a singlet-assisted version of the well-known diffusion tensor imaging technique that gives access to measurements of the full diffusion tensor of molecules diffusing within porous media with large pores. The diffusion tensor can be used to access structural information such as fractional anisotropy, pore geometry and orientation as well as tortuosity, an important parameter that has been so far inaccessible to NMR since conventional DTI fails to accurately measure it in structures with pores above 50-100 microns. Structures displaying such large pores includes battery electrodes, scaffoldings for tissue engineering, some rocks *etc*.

Acknowledgments

The authors would like to thank Monique C. Tourell for useful discussions. This research was supported by EPSRC UK grant no.: EP/N033558/1 and The Leverhulme Trust Research Project Grant no.: RPG-2019-298.

References

1. P. T. Callaghan: Translational dynamics & magnetic resonance. Oxford University Press, Oxford (2011)

2. W. S. Price: NMR studies of translational motion. Cambridge University Press, Cambridge (2009)

3. M. D. Hurlimann, K. G. Helmer, L. L. Latour and C. H. Sotak: Restricted Diffusion in Sedimentary Rocks. Determination of Surface-Area-to-Volume Ratio and Surface Relaxivity. *Journal of Magnetic Resonance, Series A*, 111(2), 169-178 (1994) doi:https://doi.org/10.1006/jmra.1994.1243

4. I. V. Thorat, D. E. Stephenson, N. A. Zacharias, K. Zaghib, J. N. Harb and D. R. Wheeler: Quantifying tortuosity in porous Li-ion battery materials. *Journal of Power Sources*, 188(2), 592-600 (2009) doi:10.1016/j.jpowsour.2008.12.032

5. E. Bullitt, G. Gerig, S. M. Pizer, W. L. Lin and S. R. Aylward: Measuring tortuosity of the intracerebral vasculature from MRA images. *Ieee Transactions on Medical Imaging*, 22(9), 1163-1171 (2003) doi:10.1109/Tmi.2003.816964

6. M. Gobel, M. Godehardt and K. Schladitz: Multi-scale structural analysis of gas diffusion layers. *Journal of Power Sources*, 355, 8-17 (2017) doi:10.1016/j.jpowsour.2017.03.086

7. S. Park, J.-W. Lee and B. N. Popov: A review of gas diffusion layer in PEM fuel cells: Materials and designs. *International Journal of Hydrogen Energy*, 37(7), 5850-5865 (2012) doi:https://doi.org/10.1016/j.ijhydene.2011.12.148

8. W. S. Price, F. Tsuchiya, C. Suzuki and Y. Arata: Characterization of the solution properties of Pichia farinosa killer toxin using PGSE NMR diffusion measurements. *J Biomol NMR*, 13(2), 113-7 (1999) doi:10.1023/a:1008394716710

9. W. S. Price, M. Nara and Y. Arata: A pulsed field gradient NMR study of the aggregation and hydration of parvalbumin. *Biophys Chem*, 65(2-3), 179-87 (1997)

10. P. W. Kuchel, A. Coy and P. Stilbs: NMR "diffusion-diffraction" of water revealing alignment of erythrocytes in a magnetic field and their dimensions and membrane transport characteristics. *Magnetic Resonance in Medicine*, 37(5), 637-643 (1997) doi:10.1002/mrm.1910370502

11. S. Mori and J. D. Tournier: Introduction to diffusion tensor imaging: And higher order models: Second edition. Elsevier Inc. \, (2013) doi:10.1016/C2011-0-07607-X

12. P. J. Basser, J. Mattiello and D. LeBihan: MR diffusion tensor spectroscopy and imaging. *Biophysical Journal*, 66(1), 259-267 (1994)

13. K. I. Momot, J. M. Pope and R. M. Wellard: Digital Processing of Diffusion-Tensor Images of Avascular Tissues. In, (2011)

14. P. J. Basser and D. K. Jones: Diffusion-tensor MRI: theory, experimental design and data analysis - a technical review. *NMR in Biomedicine*, 15(7-8), 456-467 (2002) doi:10.1002/nbm.783

15. C. Pierpaoli, P. Jezzard, P. J. Basser, A. Barnett and G. DiChiro: Diffusion tensor MR imaging of the human brain. *Radiology*, 201(3), 637-648 (1996)

16. G. Pileio: Long-lived Nuclear Spin Order: Theory and Applications. In: *New Developments in NMR*. Ed W. Price. Royal Society of Chemistry, London (2020)

17. G. Pileio, J.-N. Dumez, I.-A. Pop, J. T. Hill-Cousins and R. C. D. Brown: Real-space imaging of macroscopic diffusion and slow flow by singlet tagging MRI. *Journal of Magnetic Resonance*, 252, 130-134 (2015) doi:10.1016/j.jmr.2015.01.016

18. G. Pileio and S. Ostrowska: Accessing the long-time limit in diffusion NMR: The case of singlet assisted diffusive diffraction q-space. *J Magn Reson*, 285, 1-7 (2017) doi:10.1016/j.jmr.2017.10.003

19. M. C. Tourell, I.-A. Pop, L. J. Brown, R. C. D. Brown and G. Pileio: Singlet-assisted diffusion-NMR (SAD-NMR): redefining the limits when measuring tortuosity in porous media. *Physical Chemistry Chemical Physics*, 20(20), 13705-13713 (2018) doi:10.1039/C8CP00145F

20. E. O. Stejskal and J. E. Tanner: Spin diffusion measurements: spin echoes in the presence of a time-dependent field gradient. *The Journal of Chemical Physics*, 42(1), 288-292 (1965)

21. D. K. Jones, M. A. Horsfield and A. Simmons: Optimal strategies for measuring diffusion in anisotropic systems by magnetic resonance imaging. *Magn Reson Med*, 42(3), 515-25 (1999)

22. P. J. Basser and C. Pierpaoli: Microstructural and physiological features of tissues elucidated by quantitative-diffusion-tensor MRI. *J Magn Reson B*, 111(3), 209-19 (1996) doi:10.1006/jmrb.1996.0086

23. P. Ahuja, R. Sarkar, P. R. Vasos and G. Bodenhausen: Diffusion coefficients of biomolecules using long-lived spin states. *Journal of the American Chemical Society*, 131(22), 7498-7499 (2009) doi:10.1021/ja902030k

24. R. Sarkar, P. Ahuja, P. R. Vasos and G. Bodenhausen: Measurement of slow diffusion coefficients of molecules with arbitrary scalar couplings via long-lived spin states. *ChemPhysChem*, 9(16), 2414-2419 (2008)

25. G. Pileio, J.-N. Dumez, I.-A. Pop, J. T. Hill-Cousins and R. C. D. Brown: Real-space imaging of macroscopic diffusion and slow flow by singlet tagging MRI. *Journal of Magnetic Resonance*, 252(0), 130-134 (2015) doi:http://dx.doi.org/10.1016/j.jmr.2015.01.016

26. G. Pileio: Singlet NMR methodology in two-spin-1/2 systems. *Prog Nucl Magn Reson Spectrosc*, 98-99, 1-19 (2017) doi:10.1016/j.pnmrs.2016.11.002

27. A. H. Poonawalla and X. J. Zhou: Analytical error propagation in diffusion anisotropy calculations. *Journal of Magnetic Resonance Imaging*, 19(4), 489-498 (2004) doi:10.1002/jmri.20020

28. G. Pileio, M. Carravetta and M. H. Levitt: Storage of nuclear magnetization as long-lived singlet order in low magnetic field. *Proceedings of the National Academy of Sciences of the United States of America*, 107(40), 17135-17139 (2010) doi:10.1073/pnas.1010570107

29. M. C. D. Tayler and M. H. Levitt: Singlet nuclear magnetic resonance of nearly-equivalent spins. *Physical Chemistry Chemical Physics*, 13(13), 5556-5560 (2011)

30. G. Stevanato, J. T. Hill-Cousins, P. Hakansson, S. S. Roy, L. J. Brown, R. C. D. Brown, G. Pileio and M. H. Levitt: A Nuclear Singlet Lifetime of More than One Hour in Room-Temperature Solution. *Angewandte Chemie-International Edition*, 54(12), 3740-3743 (2015) doi:10.1002/anie.201411978

31. L. L. Latour, P. P. Mitra, R. L. Kleinberg and C. H. Sotak: Time-Dependent Diffusion-Coefficient of Fluids in Porous-Media as a Probe of Surface-to-Volume Ratio. *Journal of Magnetic Resonance Series A*, 101(3), 342-346 (1993) doi:DOI 10.1006/jmra.1993.1056

32. R. W. Mair, M. D. Hurlimann, P. N. Sen, L. M. Schwartz, S. Patz and R. L. Walsworth: Tortuosity measurement and the effects of finite pulse widths on xenon gas diffusion NMR studies of porous media. *Magnetic Resonance Imaging*, 19(3-4), 345-351 (2001) doi:Doi 10.1016/S0730-725x(01)00247-8